Exosomal cargo genes as biomarkers and potential mediators of exosome-driven cell communication in Pleural Mesothelioma

Agnieszka Kraft[1,2,3], Andrea Tönz[1,2], Fabian Schläpfer[1,2], Manuel Ronner[1,2], Vanessa Orlowski[1,2], Michaela B Kirschner[1,2], Emanuela Felley-Bosco[4#], Julia Bein[5], Peter J Wild[5], Valentina Boeva[3,6,7], Isabelle Opitz[1,2*], Mayura Meerang[1,2*]

[1]Department of Thoracic Surgery, University Hospital Zurich, Zurich, Switzerland

[2]University of Zurich, Zurich, Switzerland

[3]Department of Computer Science, Institute for Machine Learning, ETH Zurich, Zurich, Switzerland

[4]Laboratory of Molecular Oncology, Department of Thoracic Surgery, University Hospital Zurich, Zurich, Switzerland

[5]Dr. Senckenberg Institute of Pathology, University Hospital Frankfurt, Frankfurt, Germany

[6]INSERM, U1016, Cochin Institute, CNRS UMR8104, Paris Descartes University, Paris, France

[7]ETH AI Center, ETH Zurich, ZUrich, Switzerland

* shared senior authors

Present affiliation: Department of Biomedical Sciences, University of Lausanne, Lausanne, Switzerland

Abstract

Pleural mesothelioma (PM) is a rare yet aggressive and heterogeneous cancer type with very poor survival rates. Due to its long latency period and nonspecific symptoms, the disease is usually detected at advanced stages, limiting available treatment options and leading to poor survival rates. So far, the disease can only be confirmed through invasive thoracoscopic biopsy. Moreover, the proposed circulating protein biomarkers lack sensitivity and specificity, highlighting the urgent need for novel approaches.
In our previous work, we characterized the transcriptomic profile of extracellular vesicles secreted by PM cells and demonstrated their feasibility as a source of circulating biomarkers. To further investigate the role of circulating RNA in tumor progression and its potential use in non-invasive testing for PM, here we present a detailed characterization of RNA cargo carried by PM exosomes - a distinct subset of extracellular vesicles known to serve as key mediators of intercellular communication. By utilizing primary cell cultures established from

tissue samples of 11 PM and 6 non-PM patients, followed by exosome isolation, and total RNA sequencing of RNA from isolated exosomes, matching cells, and tissues, we provide new evidence on exosomal RNA secretion, regulation of PM-exosome cargo genes, and their potential functions in recipient cells. We show that PM-exosomal cargo is enriched in genes associated with proliferation, whose key transcriptional factors are *SETDB1*, *FOXM1* and *GATA2*. We identified Pcbp2, Srsf1 and Srsf9, RNA-binding proteins, which may be involved in selective cargo sorting into PM-exosomes. Our analysis identified six secreted genes, including *GAS5*, *AL031666.3*, *RSLD1D1*, *AC103740.2*, *ADAM10*, and *AC020892.1*, whose exosomal expression was associated with patient survival, as promising biomarkers for patient diagnosis, stratification, and prognosis assessment. Finally, we identify potential target genes of candidate LncRNAs biomarkers and processes in which they are involved.

Background

Pleural mesothelioma (PM) is a rare yet aggressive cancer type with very poor survival rates, ranging between 9 to 17 months after diagnosis [1–4]. The disease, associated with prior asbestos exposure in most cases [5–7], develops in the mesothelial cells composing the pleura, over a span of 30 to 40 years without manifesting symptoms [8]. This often leads to disease detection only in advanced stages and limits available treatment options. Currently standard multimodal approaches that integrate surgery, chemotherapy, and radiation, remain ineffective in many cases [8–12]. Novel approaches, including ipilimumab and anti-PD-L1 antibody, nivolumab, showed promising outcomes compared to chemotherapy, but only in patients with non-epithelioid tumors [13,14]. The difficulty of treating the disease is additionally influenced by its high molecular heterogeneity. Tumors are traditionally classified into epithelioid, sarcomatoid, or biphasic subtypes, based on the dominance of cancer cells with epithelioid or sarcomatoid morphology [15]. Of note, recent studies have shown that the histological classification does not fully explain PM heterogeneity, with intratumor transcriptional heterogeneity scores, captured by the continuum of *S*- and *E*-component marker genes expression, better capturing patient clinical characteristics [16–20].

At the same time, PM lacks non-invasive and effective diagnostic tools. Currently, non-invasive disease detection is limited to imaging-based approaches, which lack sensitivity, hence a definitive diagnosis needs to be confirmed by thoracoscopic biopsy [21,22]. Despite being very sensitive, the biopsy is an invasive procedure, not applicable for routine early screening of patients. Therefore, non-invasive and robust detection methods for PM are urgently needed.

In recent years, liquid biopsies have emerged as a promising non-invasive alternative for the detection of multiple cancer types [23–27]. Such approaches use bodily fluids, for example blood, to detect specific disease-linked biomarkers, such as tumor circulating cells, proteins, or cell-free DNA. Similar efforts have emerged for PM, with a focus on the identification of circulating protein biomarkers. While studies have shown the potential of fibulin-3, mesothelin, and osteopontin, among others, their sensitivity and specificity for routine clinical use have not been confirmed yet [28–34]. At the same time, there is a limited number of studies focusing on RNA-based biomarkers for PM. Such biomarkers are particularly

interesting, as they could shed more light on the transcriptional machinery involved in PM biology and potentially identify novel treatment targets.

Exosomes are small round-shaped endosomal vesicles, a subgroup of extracellular vesicles, secreted by all cells in an organism, including cancer cells [35,36]. They contain molecular cargo, with RNA, DNA, lipids and proteins, secreted by their donor cells. Several studies have already shown that cancer cell-secreted exosomes are shed into the bloodstream, suggesting them as a promising source of blood-based biomarkers [37,38]. Moreover, multiple studies have highlighted their role in cell-cell communication and reshaping phenotype of recipient cells [39,40]. For instance, cargo exchange between cells via extracellular vesicles has been confirmed for (1) RNAs between glioblastoma cancer cells [41], and glioblastoma and endothelial cells [42], (2) DNA sequences and retrotransposon elements between medulloblastoma and endothelial cells [43], (3) and for protein transfer between glioma cells [44]. Therefore, exosomes emerge as potential novel avenues for drug delivery systems, as well as mediators of drug resistance and disease progression [45,46]. We have previously shown that PM-derived extracellular vesicles carry RNA cargo enriched with genes associated with tumor progression, including long non-coding RNAs (LncRNAs), transcriptional factors, and marker genes of PM intratumoral transcriptional heterogeneity [47]. While our findings provide evidence for the diagnostic potential of secreted RNA cargo, the full extent of its clinical utility warrants further exploration.

In this work, we address this gap by comparing RNA cargo of exosomes secreted by PM (PM-exo) and non-PM (non-PM-exo) cells. By utilizing primary cell cultures established using pleural effusion and tissue samples from 11 PM and 6 non-PM patients, followed by exosome isolation and total RNA sequencing of RNA from exosomes, matching cells and tissues, we provide new evidence on the secretion of RNAs into PM-exosomes. We identified upregulated hallmarks of cancer associated with PM-exosome cargo, with high enrichment of genes linked to proliferation. We selected transcriptional factors, including *SETDB1*, *GATA2*, and *FOXM1*, which are potential regulators of up-secreted PM-exo genes, and whose cellular expression shows significant association with PM patient survival. Finally, we propose six secreted genes, including *GAS5*, *AL031666.3*, *RSLD1D1*, *AC103740.2*, *ADAM10*, and *AC020892.1*, as promising biomarkers for patient diagnosis, stratification, and prognosis assessment. Our comprehensive analysis provides novel insights into exosome-mediated PM biology, and proposes urgently needed biomarkers for non-invasive diagnostic approaches for PM detection.

Results

Molecular characterization of exosomes

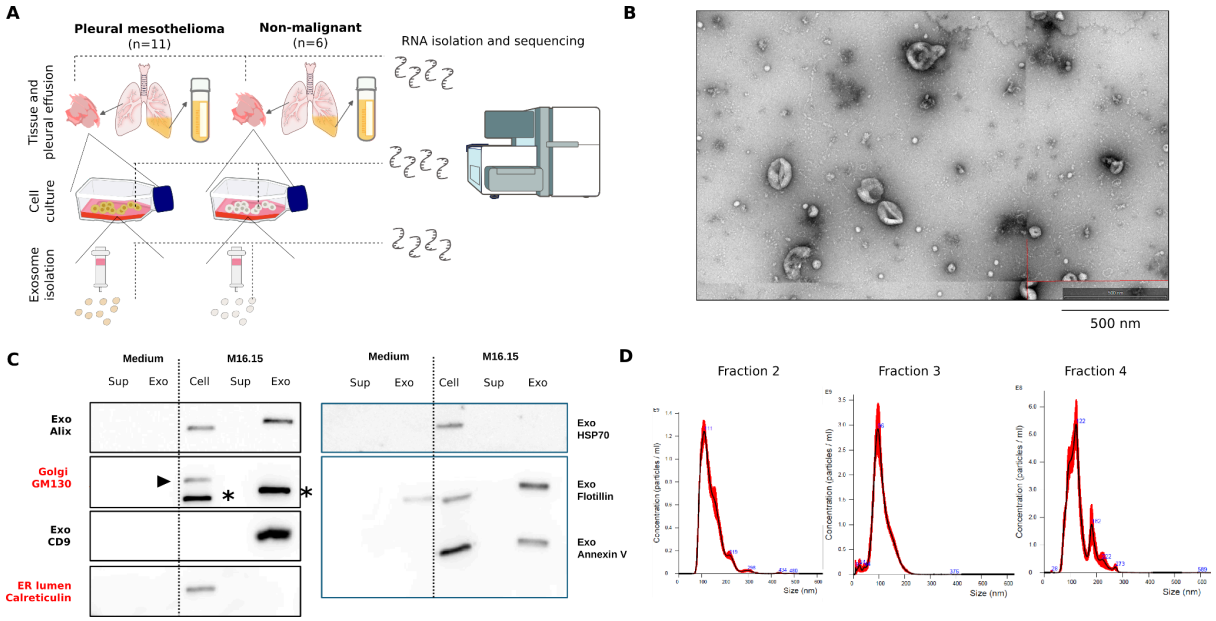

Figure 1. Exosome isolation and characterization. A. Diagram illustrating the workflow for screening exosomal RNA cargo. Tissue and pleural effusion samples from 11 PM and 6 non-PM patients were used. Tissue samples were used to establish primary cell culture. Supernatant of these cultures was used to isolate exosomes with qEV columns. RNA isolated from tissue, cells and exosomes was sequenced. **B.** Electron micrograph depicting exosomes isolated from M16.15 PM cell culture supernatant. **C.** Western blot analysis of exosomal and cellular organelle-specific proteins. Markers were tested in supernatant (Sup) and exosomes (Exo) isolated from cell culture medium and M16.15 cell culture. *remaining signal from Alix. **D.** Nanoparticle tracking analysis confirming enrichment of particles within the exosomal size range (mean diameter: 120 nm) in the collected eluate fractions from exosome isolation using qEV iZON column and M16.15 cell culture. PM - pleural mesothelioma; ER - endoplasmic reticulum.

In this work, we compared RNA cargo secreted by PM and non-PM cells, in order to identify RNA biomarkers for PM non-invasive diagnosis. To achieve this goal, we used diagnostic tissue samples and pleural effusion obtained from 11 PM and 6 non-PM, which were used to establish primary cells (Table 1, Figure 1A).

The cellular origin of cultured cells was confirmed using immunohistochemical staining of epithelial and mesothelial markers, including pan-Cytokeratin, Podoplanin, Calretinin, and Wilms' Tumor 1 (WT1) as described before [47]. To verify the agreement between genetic profiles of cultured tumor cells and matching tumors, we used Copy Number Arrays, in particular comparing the regions of *BAP1* and *MTAP*/*CDKN2A* genes, as those are often altered in PM. We found high agreement between cultured cells and the original tumors (Additional File 1). Comparison of transcriptomic profiles of these cells revealed two clusters, corresponding to PM and non-PM cells (Suppl. Figure S1A). To better characterize transcriptomic profiles of PM cells, we used previously published *S*- and *E*-component marker genes [19], and scored their expression in cells. Except for four cells, the scores corresponded to tumor histological type (Suppl. Figure S1B-C).

Table 1. Clinical characteristics of analyzed samples. Exo ID - ID of exosomal sample; Subtype - tumor histological classification; OS - overall survival time.

Exo ID	Cell ID	Tissue ID	Group	Subtype	Age	Treatment	Stage	Gender	Asbestos exposure	OS
RE41	RCD41	T41	PM	biphasic	68	Cisplatin pemetrexed	III	male	possible	26.35
RE42	RCD42	T42	PM	epithelioid	50	-	-	female	possible	40.08
RE43	RCD43	T43	non-PM	-	75	-	-	male	no	-
RE45	RCD45	T45	PM	epithelioid	68	-	IV	male	yes	1.81
RE46	RCD46	T46	non-PM	-	-	-	-	female	-	-
RE47	RCD47	T47	PM	biphasic	56	-	IV	male	yes	3.47
RE48	RCD48	T48	PM	epithelioid	69	Carboplatin pemetrexed	-	male	yes	13.07
RE49	RCD49	-	non-PM	-	-	-	-	female	-	-
RE50	RCD50	T50	PM	biphasic	65	-	III	male	yes	11.47
RE51	RCD51	T51	PM	biphasic	58	Cisplatin pemetrexed	III	male	no	15.97
RE52	RCD52	T52	non-PM	-	-	-	-	female	-	-
RE53	RCD53	T53	PM	biphasic	66	Cisplatin carboplatin pemetrexed	II	male	yes	12.78
RE54	RCD54	T54	PM	epithelioid	90	-	III	female	no	4.80
RE55	RCD55	T55	non-PM	-	-	-	-	female	-	-
RE56	RCD56	T56	PM	epithelioid	64	Cisplatin pemetrexed bevacizumab	II	male	yes	14.98
RE58	RCD58	-	non-PM	-	-	-	-	female	-	-
RE59	RCD59	T59	PM	epithelioid	84	-	II	male	yes	12.65

In the next steps, we isolated exosomes using cell culture supernatant and qEV columns (iZON), a size-exclusion chromatography technique. Purity of isolated vesicles was confirmed with Nanoparticle Tracking Analysis (NTA), by measuring the size distribution of vesicles obtained in individual qEV fractions (Figure 1D, Suppl. Figure S2). Given the highest enrichment of vesicles in the expected exosome size in fractions 2-4, vesicles from these fractions were pooled together and used for downstream analysis. Purity of exosomes was also verified by western blot analysis of exosome-specific proteins, i.e. Alix (cytosolic protein), CD9 (transmembrane protein), HSP70 (cytosolic protein), Flotillin (cytosolic protein with lipid or membrane binding capacity), and Annexin V (a phospholipid-binding protein) (Figure 1C). Their expression was tested separately in cells, supernatants, and exosomes. In addition, we tested the expression of markers associated with the Golgi apparatus matrix

(GM130) and the endoplasmic reticulum lumen (Calreticulin). As expected, exosome-specific markers were expressed in cells and exosomes, while GM130 and Calreticulin were observed only in cells (Figure 1C), confirming purity of isolated exosomes. In addition, Electron Microscopy images confirmed the expected size and morphology of isolated exosomes (Figure 1B).

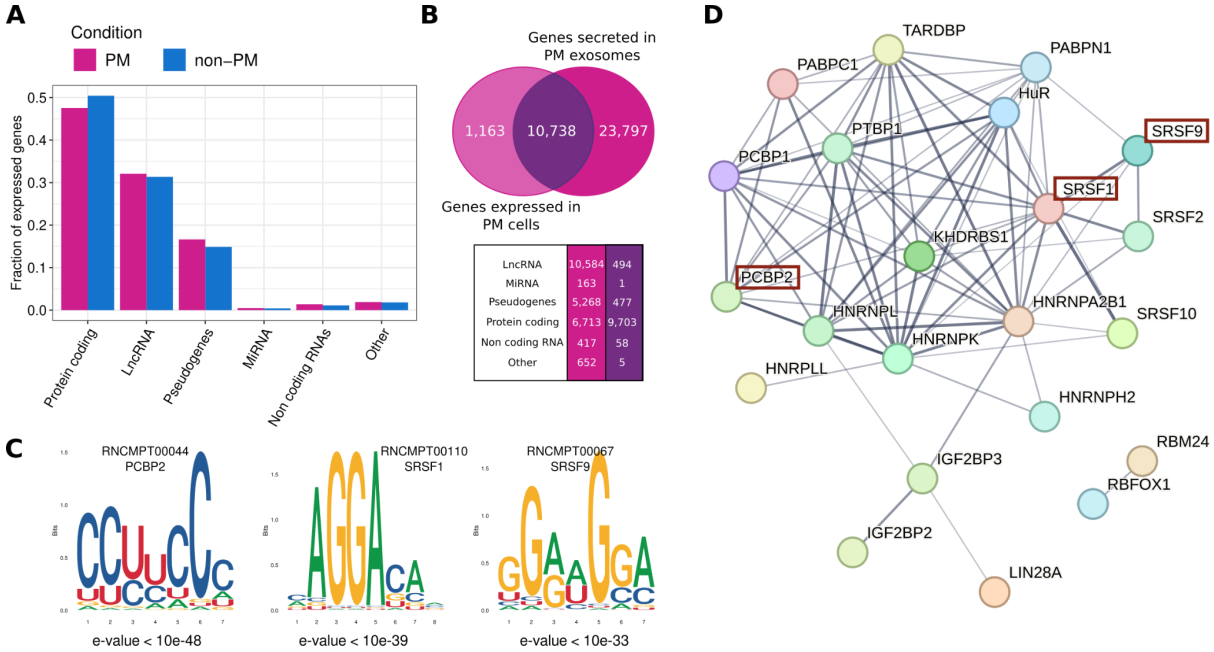

Figure 2. RNA cargo and regulatory motifs in PM-exosomes. A. Distribution of biotypes among genes expressed across all PM and non-PM exosomes. **B.** Comparison between PM-exosomal RNA cargo and genes expressed in matching PM cells. Absolute number of genes shared between exosomes and cells, or present only in exosomes, is reported in the table. **C.** Sequence logo of the three most enriched binding motifs of the PM-exo up-secreted genes. **D**. Protein-protein interactions of the RNA-binding proteins associated with significantly enriched motifs in PM-exo transcripts. Red boxes highlight the three proteins from **C**.

Transcriptomic cargo of exosomes and matching cells

In the next steps, we isolated RNA from exosomes, matching cells and tissues, and followed by RNA-sequencing (Methods). After data preprocessing, reads were mapped to the human reference genome GRCh38 and gene expression was quantified.

In total, we found 34,535 and 31,554 genes expressed across all PM-exo and non-PM-exo samples, respectively. The majority of genes in PM-exos were protein coding genes (48%), long noncoding RNA (LncRNA, 33%), and pseudogenes (18%) (Figure 2A, Suppl. Table S1). In case of non-PM exosomes, we observed a similar trend of gene biotype distribution, with a slightly higher proportion of protein coding genes (Figure 2A, Suppl. Table S1).

To gain better understanding on the link between exosomal cargo and RNAs expressed in matching cells, we analyzed distribution of gene biotypes present in cells. While in total 11,901 genes were expressed across all PM cells, over 80% of them represented protein coding genes, with significantly lower fraction of LncRNA and pseudogenes compared to exosomal samples (Suppl. Figure S3, Suppl. Table S2). Similar trend was observed in non-PM cells (Suppl. Figure S3, Suppl. Table S2).

We found 10,738 genes shared across PM-cells and PM-exos, with 1,163 genes exclusively expressed in PM-cells, and over 23,797 genes exclusively present in PM-exo (Figure 2B). As expected, the majority of the RNAs specific to PM-exo were non-coding RNAs and pseudogenes. Similar results were observed in non-PM samples (Suppl. Fig. S4), confirming higher enrichment of non-coding RNAs in exosomes compared to matching cells.

To identify potential differences in RNA cargo of microvesicles, another group of extracellular vesicles (EVs), and exosomes, we used our previous results on the RNA cargo of mixed population of EVs isolated from the same PM cells as those used in current study (Suppl. Table S3) [47]. In total, we found 11,405 genes differentially expressed between EVs and exosomes, with 817 genes upregulated and 10,588 downregulated in exosomes (log2 fold change threshold 1 and -1, p-value < 0.05, Suppl. Fig. S5). Interestingly, the downregulated genes in exosomes were mostly protein-coding genes (9,675 genes; Suppl. Table S4).

RNA-binding proteins involved in PM-exosome cargo sorting

Given the observed varied distribution of detected genes in matching EVs, exosomes and cells, we investigated the potential mechanism of selective cargo sorting into exosomes. Specifically, we used Analysis of Motif Enrichment (AME) from the MEME suit [48], to analyze the enriched RNA-binding motifs in PM-exo genes. We found strong enrichment of 42 motifs (e-value < 0.05) associated with several RNA-binding proteins (Suppl. Table S4). Among top significant hits, we found CU-rich motifs bound by Pcbp2, and GGAG-rich motifs, bound by Srsf1 and Srsf9 (Figure 2C). Srsf1 has been previously shown to mediate selective sorting of microRNA into exosomes in pancreatic and breast cancer cell lines [49], while Pcbp2 has been associated with higher microRNA secretion via EVs, leading to EGFR-driven angiogenesis [50]. Both Srsf1 and Srsf9 binding was shown to promote Beta-catenin accumulation in cancer cells, which promoted Wnt signalling [51].

Additionally, we used the STRING database [52], which collects experimentally verified protein-protein interactions, to identify additional proteins involved in the PM-exo cargo sorting and interacting with identified RNA-binding proteins. We identified 13 additional proteins highly interacting with Pcbp2, Srsf1 and Srsf9, including hnRNPA2B1, previously shown to regulate microRNA loading into exosomes [53] (Figure 2D).

Transcriptomic comparison of PM and non-PM-exosomes

Given the growing evidence of exosomes as a source for disease biomarkers, we compared the transcriptomic cargo of exosomes secreted by PM and non-PM-cells. Overall, 3,204 and 1,103 genes were up- and down-expressed in PM-exo compared to non-PM-exo samples (Figure 3A, p-value < 0.05, Suppl. Table S5). Among top enriched genes, we found four *S*-component and three *E*-component genes (Suppl. Figure S6A), along with 20 transcriptional factors (Suppl. Figure S6C), 16 enriched microRNAs (Suppl. Figure S6B) and 720 LncRNAs (Suppl. Figure S6D, Suppl. Table S5). Interestingly, among the up-secreted LncRNAs we found *GAS5* and *POT1-AS1*, previously identified as potential blood-based biomarkers for epithelioid PM [54]. In addition, *ABCA5*, *ABCA10* and *ABCA9-AS1*, which represent ABC-transporter genes (Suppl. Fig. S6E), previously associated with the multidrug resistance phenotype [55], were among the up-regulated genes.

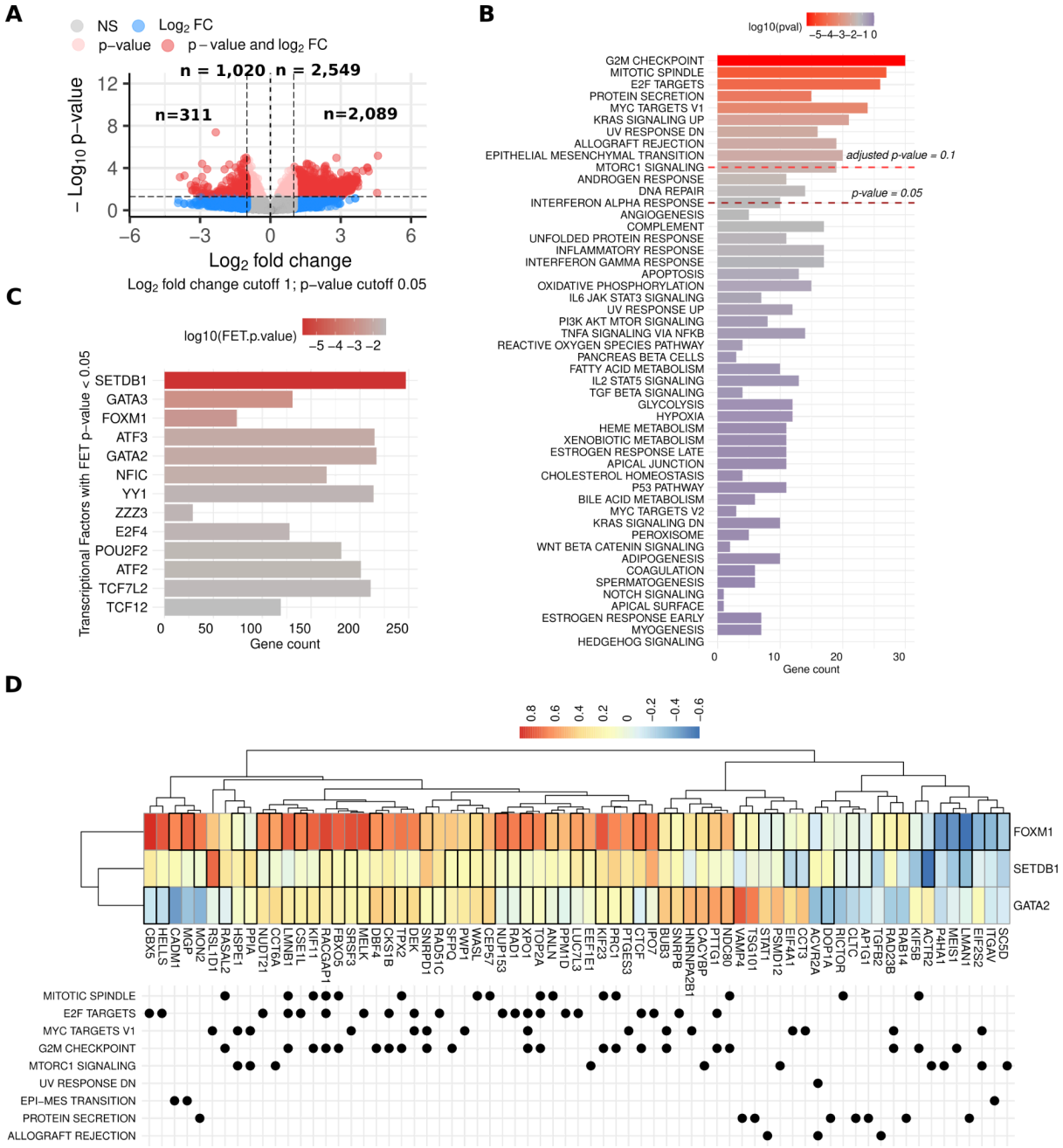

Figure 3. Functional and regulatory landscape of PM-exosomal cargo. A. Differential gene expression between PM and non-PM exosomal cargo. **B.** Hallmarks of cancer in which PM-exo up-regulated genes are involved. **C.** Top 10 transcriptional factors with the strongest enrichment of PM-exo up-secreted genes. **D.** Correlation between expression of the top three most enriched transcriptional factors and their target genes expression in PM cells. Color scale represents Pearson's correlation coefficient. For each target gene, hallmarks of cancer in which it is involved is marked below the heatmap.

Hallmarks of cancer enriched in PM-exosomes

To understand processes in which PM-exosome enriched genes are involved, we used gene set enrichment analysis to verify their association with hallmarks of cancer from MsigDB. We

found significant enrichment of 13 hallmarks (p-value < 0.05), with *G2M Checkpoint*, *Mitotic spindle formation*, and *E2F targets* among the top enriched pathways (Figure 3B).
In the next steps, we scored exosomal expression of the genes involved in the top enriched hallmarks, as well as up-secreted *S*- and *E*-component genes, to assess the link between exosomal activity of these pathways and PM patients' survival. For each score, we used a multivariate Cox regression model along with tumor histological subtype and treatment information (Table 1). Higher scores of seven pathways were associated with worse patient prognosis, with the highest hazard linked with *UV response down* set (Suppl. Figure S7). Interestingly, *Epithelial-Mesenchymal Transition* (EMT)-related score was associated with better patient prognosis, contrary to the growing evidence on the link between EMT and cancer progression [56]. In parallel, we scored the expression of the same genes in PM cells, and repeated Cox regression analysis to assess the link between cellular activity of these pathways and patient survival (Suppl. Fig. S9). Four sets, i.e. *MYC targets*, *MTORC1 signaling*, *E-component*, and *E2F targets*, showed association with higher hazard, while three sets, i.e. *Allograft rejection*, *KRAS signaling up*, and *EMT*, were linked with lower hazard, consistent with results found for exosomes. Interestingly, higher levels of *UV response down*-related genes in PM cells were linked with better survival, contrary to their link with higher hazard based on exosomal expression (Suppl. Figure S7-S8).

Transcriptional regulators of PM-exosomal RNA cargo

To identify potential transcriptional factors (TF) regulating expression of PM-exo enriched genes, we used ChEA3 [57], which provided enrichment scores of TFs with experimentally verified binding sites to promoter regions of PM-exo enriched genes. We obtained 13 TFs with significant enrichment (FET p-value < 0.05, Suppl. Table S7), with *SETDB1*, *GATA3* and *FOXM1* among the top enriched factors, targeting respectively 248, 127 and 75 genes expressed in PM-exos (Figure 3C, Suppl. Table S7). From the set of 13 enriched TF, cellular expression of *SETDB1*, *FOXM1* and *GATA2* was significantly linked to patient survival (Cox multivariate regression analysis with subtype and treatment information, p-value < 0.05, Suppl. Figure S9). *GATA2* was predominantly positively correlated with expression of its targets, mostly involved in proliferation, i.e. *MYC targets V1*, *E2F targets*, and *G2M checkpoint* (Figure 3D). *FOXM1* was the only TF regulating genes involved in EMT, with strong positive correlation, while both *FOXM1* and *SETDB1* negative regulated genes involved in *mTORC signaling* (Figure 3D).

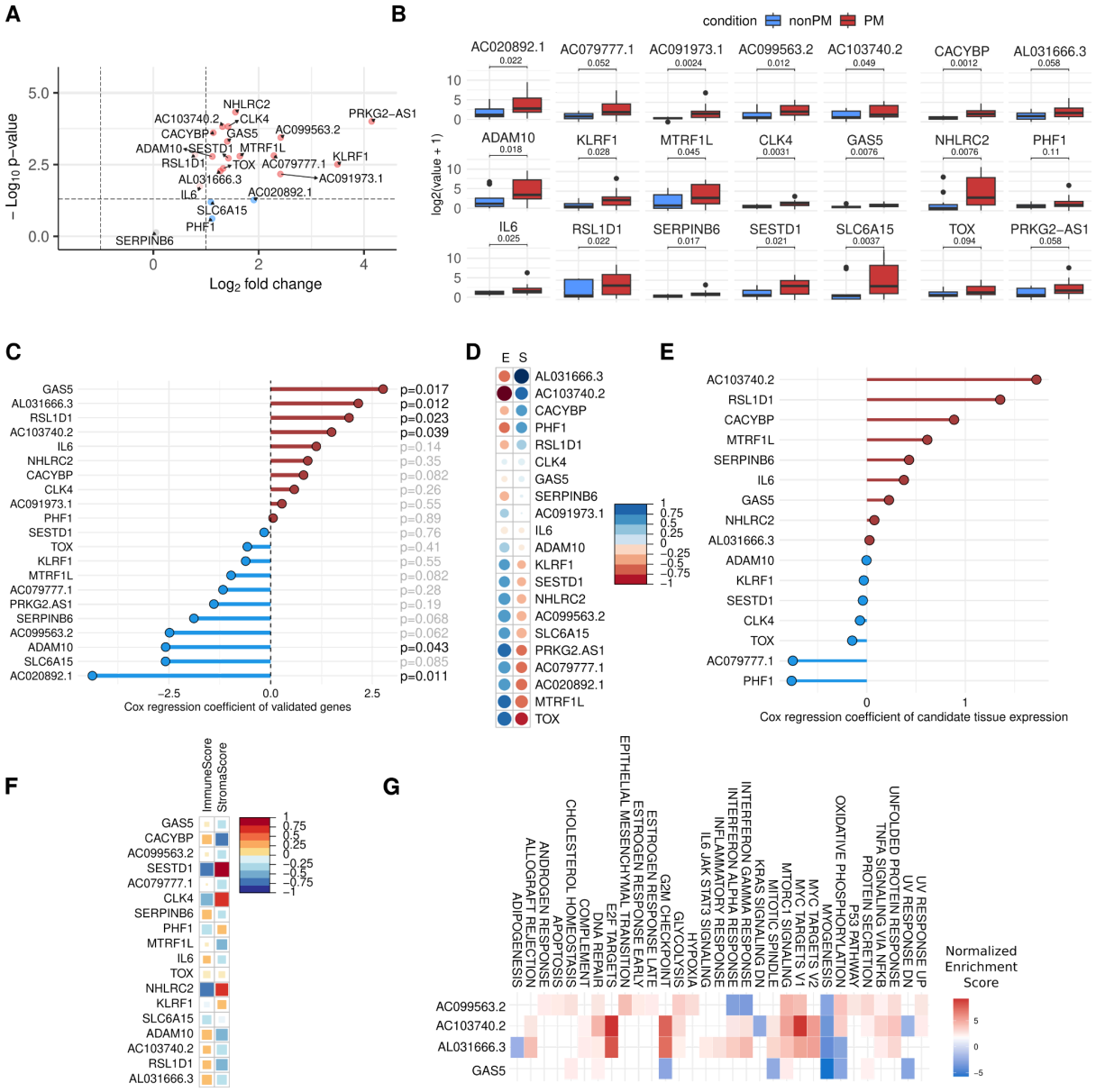

Figure 4. Exosomal candidate genes for PM detection. A. Volcano plot generated using sequencing data of qPCR-validated candidate genes. **B**. RT-qPCR validation of PM-exo candidate genes in technical replicates of exosomes. Significance was computed using Mann-Whitney U-test. **C.** Cox survival analysis using exosomal expression of validated candidate genes (multivariate models with histological type and treatment). **D.** Correlation between exosomal expression of candidate genes and *S-/E*-compartment scores of matching PM cells. **E.** Cox survival analysis of candidate genes in PM tissue expression data. **F.** Correlation between PM tissue expression of candidate genes and xCell Immune and Stromal scores. **G.** Hallmarks of cancer enriched with predicted targets of validated long non-coding RNA genes.

Technical validation of candidate RNA biomarkers using RT-qPCR

Next, we selected 30 candidate genes for technical validation using technical replicates of PM and non-PM cell cultures whose secreted exosomes were profiled with RNA-sequencing (Suppl. Figure S10). We repeated exosome isolation from the technical replicates of primary cells, isolated exosomal RNA, and used quantitative reverse transcription polymerase chain

reaction (RT-qPCR) to validate the enrichment of selected genes in PM- vs. non-PM-exo. The analysis confirmed significantly higher expression of 7 LncRNA and 14 protein coding genes in PM compared to non-PM exosomes (Figure 4A-B, Suppl. Table S6, S8; Mann-Whitney p-value < 0.1).

Six of the validated genes showed significant association with patient survival (Cox regression p-value < 0.05, models including histological subtype and treatment information, Figure 4C). The validated genes in general had higher expression in epithelioid tumors compared to biphasic ones (Suppl. Fig. S11), with five candidates, *AL031666.3*, *AC103740.2*, *CACYBP*, *PHF1* and *RSLD1,* were positively correlated with *E*-scores of matching cells. Conversely, ten genes, *KLRD1*, *SESTD1*, *NHLRC2*, *AC099563.2*, *SLC6A15*, *PRKG2-AS1*, *AC079777.1*, *AC020892.1* and *TOX*, were positively correlated with *S*-component scores (Figure 4D).

Potential role of PM-exosomal RNA cargo in the tumor microenvironment

In the next steps, we used RNA-sequencing data from exosome-matching tissue samples, to assess the clinical and functional role of validated PM-exo genes in the tumor microenvironment (TME). The expression of *CACYBP*, *AC103740.2*, and *RSL1D1* was predictive of patient survival, in both univariate and multivariate models with subtype information (Figure 4E, Suppl. Table S9). Survival analysis using TCGA mesothelioma data confirmed results for the two first genes, and revealed three additional genes with significant association (Cox univariate p-value < 0.05, Suppl. Fig. S12).
In the context of TME composition of PM tissues, we found an association between tissue expression of several candidate genes with either immune or stromal scores, reflecting the infiltration of the respective cell types. Specifically, *SESTD1*, *CLK4* and *NHLRC2* showed the strongest correlation with stroma scores, with *CACYBP*, *SERPINB6*, *IL6*, *ADAM10*, *AC103740.2*, *RSL1D1* and *AL031666.3* positively linked to immune scores (Figure 4F). We observed similar patterns of association in TCGA mesothelioma data (Suppl. Fig. S13). Interestingly, several of the genes, in particular *AC103740.2* and *TOX*, were also positively correlated with PD-L1 protein expression as well as CD274 gene expression in TCGA tissue samples, suggesting they could potentially be further explored for immunotherapy patient stratification (Suppl. Fig. S14). In addition, we found four genes with significant differences in gene expression across tumor subtypes (Suppl. Table S10, Figure S19), as well as higher expression of *AC103740.2* associated with better response to chemotherapy in TCGA mesothelioma samples (Suppl. Fig. S15).
Finally, using PM tissue gene expression, we identified potential protein coding target genes of four validated LncRNA biomarkers, which were enriched with over 30 different hallmarks of cancer (adjusted p-value < 0.01, Figure 4F). The target genes presented the strongest enrichment of *E2F targets*, *G2M checkpoint*, and *MYC targets V1* pathways, and negative enrichment of *Myogenesis, Oxidative phosphorylation*, and *UV response down*, which suggest they could be potential co-activators and repressors of these respective processes in PM-exosome-recipient cells.

Discussion

Exosomes, previously explored in other cancer types and highlighted as important mediators of tumor progression and cellular cross-talk, have not yet been fully investigated in PM. Our analysis, which integrates transcriptomic data from exosomes secreted by PM and non-malignant cells complemented with RNA-sequencing data from matching cells and tissues, allowed us to explore exosome-mediated PM biology at multiple levels.

First, as previously reported, we observed a higher proportion of non-coding RNAs in exosomes compared to matching cells, emphasizing their role as potential mediators of post-transcriptional regulation in recipient cells [58–60]. When comparing genes secreted into PM exosomes and mixed population of extracellular vesicles, we found higher expression of protein coding genes in the mixed population, suggesting that exosomal and microvesicle cargo may be sorted using different principles, therefore may have distinct functions in recipient cells.

Second, we identified several RNA-binding proteins that may be involved in selective sorting of RNAs into exosomes. Among the most associated RNA-binding proteins, we found Pcbp2, Srsf1 and Srsf9, previously linked with microRNA binding and secretion in cancer cells [49][50][51]. Since exosomal RNA cargo can contain molecules capable of inducing pro-oncogenic changes in recipient cells, identifying proteins involved in its sorting could be crucial for future targeting of pathways regulating their secretion.

Third, the comparison between exosomes secreted by PM and non-malignant mesothelial cells, allowed us to identify over 2,000 genes with higher expression in PM, including transcriptional factors and non-coding RNAs. We confirmed 21 candidate biomarkers, including long noncoding RNAs and protein-coding genes, such as *GAS5*, *ADAM10*, *AL031666.3*, *RSLD1D1*, *AC103740.2*, and *AC020892.1,* using an orthogonal experimental approach. Importantly, exosomal expression of these genes was significantly linked with patient survival in our cohort, and several of them were correlated with scores characterizing PM-specific intratumor transcriptional heterogeneity.

The exact role of exosomal cargo in cancer has not been fully explored yet, however, there are two main hypotheses. One suggests that the cargo consists mostly of cellular by-products destined for removal, while the other suggests that RNAs are selectively sorted into exosomes for intercellular communication. To explore these hypotheses, we analysed enriched pathways in which PM-exo genes are involved, as well as their association with patient survival. Overall, PM-exo cargo was enriched with hallmarks of proliferation, suggesting that exosomes could potentially transfer proliferation-linked phenotypes into their recipient cells. While we have not tested the functional role of the cargo in recipient cells, the already published evidence supports its potential role in modulating phenotype of recipient cells [39,61].

Finally, we explored the potential effects of the validated candidates in recipient cells in TME. We identified several genes that could be targeted by enriched LncRNAs in tissue samples, and processes in which they are involved. The analysis showed that *AC103740.2*, *AL031666.3* and *AC099563.2* may promote proliferation, while *GAS5* could be linked with decreased activity of oxidative phosphorylation, both processes important for tumor

progression. Moreover, *AC103740.2* expression in tissue was associated with higher immune TME scores, suggesting it might have higher expression in immune-rich tumors. This was consistently observed in both our cohort and TCGA mesothelioma data. In addition, its expression in TCGA data was associated with PD-L1 expression, suggesting it could potentially be used as a biomarker for immunotherapy patient stratification.

Our study has several limitations. First, our analysis was limited to tumors with epithelioid and biphasic subtypes, potentially limiting the power of identifying biomarkers of sarcomatoid subtype. However, we observed that the molecular classification of tumours did not directly correspond to the enrichment of *S*- and *E*-scores of matching PM cells, with our results showing that some cells originating from epithelioid tumors presented high expression of the sarcomatoid-like component, and vice versa. Therefore, we believe that the identified biomarkers are universal for PM detection across histological subtypes. Second, our analysis on the proteins involved in cargo sorting, transcriptional factors regulating PM-exo genes, and functional effects of PM-exosome on recipient cells, should be verified experimentally to validate their involvement in these processes. Third, extensive validation of the identified biomarkers in large cohorts of plasma samples is necessary to confirm their diagnostic and clinical potential.

Despite these limitations, our work presents new insights on exosomes secreted in pleural mesothelioma. It is the first work to characterize their RNA composition and evaluate their clinical significance in the context of matching cells and tissue samples. Our findings provide new evidence on the role of exosomal RNA in PM biology and highlight their potential as a source for non-invasive circulating biomarkers.

Materials and methods

Cell cultures

Primary cell cultures of 9 pleural mesothelioma and 6 non-malignant mesothelial cells were established using treatment-naive pleural effusion samples of patients undergoing diagnosis at the Department of Thoracic Surgery, University Hospital Zurich (Table 1). Two cell cultures were isolated from PM tumor tissues as previously described, SDM90 and SDM134 [62]. Pleural effusion samples were processed as described previously (ref our paper)and cell cultures were maintained at 37 °C and 5% CO_2 and verified to be free from mycoplasmas. To identify the identity of the cells, we performed immunohistochemical staining of protein markers as described previously [47] and copy number variation array. Four PM and 2 non-PM cell lines were validated previously [47]. The verification of additional cell lines used in this study is provided in the Additional File 1.

Exosome isolation

Cells were seeded in the complete medium in 10 of 150 cm^2 non-coated cell culture dishes until reaching 50–70% confluency. Cells were then washed three times with 15 ml DPBS to clean exosome contamination in the FBS. After that, 20 ml of the culture media, RPMI medium ATCC modification (GibcoTM, A1049101, Life Technology Europe BV, Zug, Switzerland) containing 2mM glutamine (Sigma-Aldrich Buchs, Switzerland), human

Epidermal Growth Factor (20 ng/ml, hEGF) and 8% exosome depleted FBS (Life technology A27208-03) was added to each dish. After 72 h incubation, we collected the all 20 ml supernatant and cells were washed again with 10 ml DPBS to collect the remaining medium. The total volume of 300 ml supernatant plus DPBS was collected from each cell culture. The medium was centrifuged at 400 g for 5 min at 4ºC to sediment cells. The supernatant was subjected to the next centrifugation again at 3,000 g for 15 min at 4ºC to remove large debris. Afterwards, the supernatant was filtered through a 0.22 µm vacuum filtration device (TPP, 99250). The supernatant was further concentrated to a total volume of 4 ml using Centricon Plus-70 PL-100 100k (Millipore UFC710008). The concentrate was again centrifuged at 10,000 g for 10 minutes at RT to remove debris. Afterwards, we performed exosome isolation using iZON qEV1/35 nm (iZON Science) following manufacturer's guidelines using loading volume of 1 ml. We collected and pooled fraction 2-4 as these are enriched with exosomes (supplementary figure X). The exosome isolation was repeated 4 times using the same iZON column with in between washing with 1 column volume (14 ml) of DPBS. Exosomes solution was either directly used for NTA and electron microscopy. For RNA and protein isolation, we added 800 ul Nanotrap® EV Particles (RNA concentration kit, iZON Science) in 8 ml exosome eluate, incubated and rotated at room temperature for 1 hour. After that, the samples were centrifuged at 16,800 g for 10 minutes and the supernatant was discarded. The remaining Nanotrap® pellets bound to exosomes were snap frozen and stored at -80°C until further analysis.
In addition to exosomes, we also collected the cells (from 1 dish) by trypsinization and counted the number of cells and verified the cell viability of >80% for all samples. Cells were washed twice in DPBS and snapped frozen for RNA isolation.

Western blot analysis

Nanotrap® pellets bound to exosomes or cells were lysed with cell lysis RIPA buffer (50 mM Tris HCl pH. 8, 150 mM NaCl, 1% TritonX-100, 0.5% sodium deoxycholate, 0.1% SDS) containing protease/phosphatase inhibitor cocktail (Cell Signaling, #5872, Danvers, MA, USA). For supernatant we used 4 ml of supernatant and concentrated using Amicon Ultra 4 ml 3K Preparation of cell extract and western blot, we performed as we previously described [47]. We used the primary and secondary antibodies from exosomal marker antibody sampler Kit (Cell Signaling, Danvers, MA, USA, #74220) to detect the expression of exosomal markers and markers for possible contamination from released organelles including Golgi and Endoplasmic reticulum.

Copy Number Analysis

We isolated DNA from primary cell cultures using Qiagen DNeasy Blood & Tissue mini Kits (69504, Qiagen Hombrechtikon Switzerland). DNA from tumor tissues were isolated by Qiagen FFPE DNA isolation kit (56544, Qiagen). PM primary cells and matched tissue samples were characterized using Affymetrix OncoScan Microarray according to the instruction manual (Applied Biosystems, 902695). Obtained CEL files were analyzed using Analysis Power Tools (Thermo Fisher, version 2.4.0) and rCGH R package. The results of the analysis are presented in Additional File 1.

Nanoparticle Tracking Analysis

Nanoparticle Tracking Analysis was performed using NanoSight (NS300-Malvern).

Electron Microscopy

5 µl of elute from the iZON qEVoriginal column was applied to a glow-discharged grid of 300 mesh copper and incubated for 1 minute. Excess liquid was removed and then stained with , with 2% uranyl acetate for 1 min. The slide was dried and subjected to imaging by transmission electron microscopy.

RNA isolation

We used *mir*Vana PARIS Kit (Ambion #AM1556) for RNA isolation. We added 625 ul ice cold cell disruption buffer to the cell pellet, after vortexing we added equal volume of Phenol-Chloroform to the sample and proceeded with totalRNA isolation according to the instruction manual. Nanotrap® pellets bound to exosomes were resuspended in 400 ul ice cold cell disruption buffer. After vigorous vortexing, the sample was centrifuged at 16,800 g, 4ºC for 10 minutes. The supernatant was collected for RNA isolation and the equal volume of Phenol-Chloroform was added followed by RNA isolation. For tumor tissues, we used tissue samples frozen in optimal cutting temperature (OCT) medium. We performed tissue sectioning (10 um) with a microtome. Tissue sections were lysed with 625 ul ice cold cell disruption buffer and proceed as for RNA isolation from cells. From 2 samples (SDM90 and SDM76), the RNA were previously isolated with the RNeasy kit (Qiagen). A total of 85 ul RNA eluate was obtained from the *mir*Vana PARIS kit. RNA concentration was measured by Qubit™ RNA High Sensitivity assay Kit (Invitrogen, Q32852). RNA concentration from exosome samples were below the detection limit despite the use of the high sensitivity kit. The RNA from cells and tissues were treated with DNAse prior to library preparation using TURBO DNA-free™ Kit (Ambion AM1907) according to manufacturer's instructions. RIN number of RNA was measured by bioanalyzer device using Eukaryote Total RNA Pico kit ensuring RIN>7 for all tissue samples with the exception of M21.04, M16.25 and M19.36.

Preparation of libraries

As starting material, we used 5 ng of DNase treated RNA extracted from cells or tissues in a total volume of 7 µl. For exosomal RNA, we used a total of 7 µl of RNA suspension as the starting material from all samples, because the RNA concentration was below the detection limit. For all samples, we performed 6 minutes of RNA fragmentation. We used SMART-Seq Stranded Kit (Takara, 634444), together with the SMARTer RNA Unique Dual Index Kit – 96U Set A, (634452) for the indexes. We used 5 cycles for PCR-1 step and 13 cycles for PCR-2 step. One final clean up step was applied. Library size was verified using bioanalyzer. Library preparation was conducted for cell culture medium (negative control), where no library amplification was detected.

RNA-sequencing data analysis

All libraries were pooled and sequenced using a Novaseq6000 SP(100) in one S4 lane, to obtain paired-end 150 bp reads. Data was sequenced at the Genomics Facility Basel. Quality of obtained reads were accessed using FastQC (https://www.bioinformatics.babraham.ac.uk/projects/fastqc/, version 0.11.9). Reads were processed using fastp [63] to remove adapter sequences and perform quality-based read trimming. Processed reads were mapped to the human reference genome GRCh38.p13 using STAR (https://github.com/alexdobin/STAR; version 2.7.5c). STAR-inferred gene counts were used for downstream analysis. Annotation of transcriptional factors was obtained from the FANTOM5 database (https://fantom.gsc.riken.jp/5/). *S*- and *E*-component marker genes were obtained from [19]. For UMAP visualisation of cells, calculated using the UMAP R package [64], data was normalized using Variance Stabilized Transformation (vst) function from the DESeq2 R package [65].

Enrichment of RNA-binding proteins

Sequences of the longest transcripts of the PM-exosome expressed genes were obtained from the gencode GTF file (version 35). Analysis of Motif Enrichment from MEME suite [48] was used along with the Ray2013 database of RNA-binding proteins, to identify proteins whose binding motifs are enriched in the PM-exo transcripts, with transcripts expressed in matching PM-exo cells as as background set. Identified proteins whose motifs had significant association (p-value < 0.05) were provided to the STRING database [52] to identify interacting proteins based on experimental data and medium interaction confidence (score > 0.4).

Differential gene expression analysis

Genes upregulated in PM-exosomes compared to non-PM-exosomes were identified using differential gene expression analysis with the DESeq2 R package [65]. For the biotype analysis of expressed genes, the gencode GTF file (version 35) was used.

Gene set enrichment analysis

Gene set enrichment of the upregulated PM-exosome genes was calculated using hallmarks of cancer from MsigDB (https://www.gsea-msigdb.org/gsea/msigdb/) and hypergeometric test from the fgsea R package (https://bioconductor.org/packages/release/bioc/html/fgsea.html). *S*- and *E*-compartment scores of PM cells, tissue, TCGA expression, as well as scores of selected enriched pathways in exosomes, were calculated using the ssgsea [66] method from the GSVA R package.

Analysis of Transcriptional Factors

Chea3 (https://maayanlab.cloud/chea3/) was used to identify transcriptional factors whose experimentally validated targets were enriched in the PM-exosome enriched genes. For evaluation of regulation effect on target genes, we summed normalized counts from

exosomes and matching cells, as total expressed genes, and correlated these values of the PM-exosome enriched genes with the transcriptional factors identified with Chea3.

Survival analysis

Cox regression analysis implemented in the survival R package was used to assess association with survival. Multivariate models were trained using respective genes or scores calculated for cells, exosome or tissue samples, along with tumor subtype and treatment, provided in Table 1. For TCGA mesothelioma data, tumor subtype information was used in multivariate models.

RT-qPCR analysis

We used Prelude One-Step PreAmp Master Mix (Takara Bio, 638553) optimized for unbiased co-amplification to pre-amplify the cDNA generated from exosomal RNA to increase the detection sensitivity. For gene specific preamplification, the final concentration of each primer was 50 nM in a total volume of 25 ul reaction. As starting material, 5 µl of RNA solution from the miRVANA PARIS kit eluate was used. The preamplification was performed using the following cycling condition for each primer mix: 42°C 10 minutes, 95°C 2 minutes, 14 cycles of 95°C10 second and 60°C for 4 minutes. Using this reaction setting, high efficacy of pre amplification was observed (Ct Preamp- Ct without Preamp > 10 cycles). For qPCR, we diluted the preamplification reaction to at least 1:2.2 dilution with ultrapure water. A positive control (RNA isolated from cells) and no template control (ultrapure water) were included in every set of preamplification. Three µl of the diluted sample was used for quantitative real-time PCR (qPCR) in at least technical duplicates, using KAPA SYBR FAST qPCR master mix with low ROX (Kapa Biosystems, KK4621 Merck, Buchs, Switzerland) in a 10 µl reaction volume containing 200 nM of each primer, using the same instrument and setting as previously described. No template control for qPCR reaction was conducted. cDNA from no-preamplification was run on every plate for the comparison of melt curve analysis. We assumed a reaction efficiency of 100%. To normalise the expression data we selected genes that showed no difference in the expression between PM-exo and non-PM-exo, and gene candidates previously proposed as reliable and stable housekeeping genes for exosomes [67]. Among the selected genes, we identified OR2V2, OST4 and SNPRG that showed no significant difference in Ct between PM and non-PM exosomes (Suppl. Fig. S20). In addition, we observed a tendency of negative correlation between cell number and Ct value of these genes (Supp. Fig. S21). Gene expression was quantified using $\mathbf{2}^{-\Delta\Delta CT}$ method normalized with average Ct of the reference genes (OST4, SNRPG, and OR2V2) using mean ΔCt of non-PM exosome samples as reference value. OR2V2 was included in all the primer mix to ensure the consistent preamplification efficiency of every preamplification. Primers used are listed in Suppl. Table S11.

Comparison between matched EV and exosome RNA cargo

We used extracellular vesicle RNA-seq data from [47] to compare RNAs present in EVs and exosomes secreted from matching cells. ID matching of the EV and exosome samples can be found in Suppl. Table S3. For this comparison, the expression of the exosome samples was calculated using Kallisto (https://pachterlab.github.io/kallisto/download.html; version

0.46.1) as described before [47]. Then, EV and exosome expression was batch-normalized using the Qsmooth R package (https://bioconductor.org/packages/release/bioc/html/qsmooth.html). Differential gene expression was analyzed using DESeq2 R package [65].

TCGA mesothelioma data analysis

STAR counted and FPKM-UQ normalized RNA-seq data from GDC TCGA mesothelioma dataset was downloaded from UCSC Xena browser (https://xenabrowser.net/datapages/). Log2 transformation was reversed, and used for downstream analyses. For clinical association analysis, clinical and treatment information linked to the dataset was obtained using TCGAbiolinks R package following the instructions from user manual [64,68]. The significance of associations was tested using Kruskal-Wallis test. The normalized RPPA expression of PDL1 for correlation analysis with gene expression of PM-exo genes, was downloaded from UCSC Xena browser (https://xenabrowser.net/datapages/).

Tumor Microenvironment Scores

The scores representing infiltration of immune and stromal cell types of TCGA mesothelioma and PM tissue samples was calculated using xCell [69].

Candidate targets of validated long noncoding RNAs

PM tissue expression data was used to identify potential target genes and pathways of PM-exo enriched LncRNAs. The expression of validated LncRNAs was correlated with the expression of all expressed protein-coding genes in PM tissue samples. For each LncRNA, the target genes were ordered based on decreasing correlation with its expression, and the ordered list of genes was used for enrichment analysis using fgsea R package (https://bioconductor.org/packages/release/bioc/html/fgsea.html) and hallmarks of cancer sets (https://www.gsea-msigdb.org/gsea/msigdb/). Only hallmarks with adjusted p-value < 0.01 were reported.

Acknowledgements

We sincerely thank Dr. Emanuela Felley-Bosco for providing samples originating from SDM90 and SDM134 tissues.

Funding

This work was supported by the Swiss National Science Foundation grant “Improving Mesothelioma Patients Outcomes by Early Non-Invasive Diagnosis” (grant number 32003B_176063), Schweizerische Unfallversicherungsanstalt (SUVA) grant “Biomarkers for early detection of malignant pleural mesothelioma” and Stiftung für angewandte Krebsforschung (SAKF).

Author information

Competing interests

IO discloses the following: No real conflicts of interest. The following could be perceived as such: Roche (Institutional Grant), AstraZeneca (Advisory Board), MSD (Advisory Board), BMS (Advisory Board), Medtronic (Institutional Grant and Advisory Board), Intuitive (Proctorship and Speakers Fee), Sanofi (Speakers Fee), Regeneron (Advisory Board), XVIVO (Institutional Grant), Siemens (Speakers Fee), Astellas (Speakers Fee). IO is International Director for AATS, Member of the Thoracic Clinical Practice Standards Committee and the Thoracic Education Committee of AATS, ESTS Board Member, iMig Board Member and JTCVS Associate Editor.
The remaining authors declare no competing interests.

Ethics declarations

All procedures involving pleural mesothelioma primary cultures were approved by the Ethics Committee of the canton Zurich on 09/02/2021 with the approval number BASEC-Nr. 2020–02566.

References

1. Popat S, Baas P, Faivre-Finn C, Girard N, Nicholson AG, Nowak AK, et al. Malignant pleural mesothelioma: ESMO Clinical Practice Guidelines for diagnosis, treatment and follow-up. Ann Oncol. 2022;33: 129–142.

2. Janes SM, Alrifai D, Fennell DA. Perspectives on the Treatment of Malignant Pleural Mesothelioma. N Engl J Med. 2021;385: 1207–1218.

3. Vogelzang NJ, Rusthoven JJ, Symanowski J, Denham C, Kaukel E, Ruffie P, et al. Phase III Study of Pemetrexed in Combination With Cisplatin Versus Cisplatin Alone in Patients With Malignant Pleural Mesothelioma. J Clin Oncol. 2023;41: 2125–2133.

4. Christoph DC, Eberhardt WEE. Systemic treatment of malignant pleural mesothelioma: new agents in clinical trials raise hope of relevant improvements. Curr Opin Oncol. 2014;26: 171–181.

5. Pinato DJ, Mauri FA, Ramakrishnan R, Wahab L, Lloyd T, Sharma R. Inflammation-based prognostic indices in malignant pleural mesothelioma. J Thorac Oncol. 2012;7: 587–594.

6. Visonà SD, Bertoglio B, Favaron C, Capella S, Belluso E, Colosio C, et al. A postmortem case control study of asbestos burden in lungs of malignant mesothelioma cases. J Transl Med. 2023;21: 875.

7. Spirtas R, Heineman EF, Bernstein L, Beebe GW, Keehn RJ, Stark A, et al. Malignant mesothelioma: attributable risk of asbestos exposure. Occup Environ Med. 1994;51: 804–811.

8. Ray M, Kindler HL. Malignant pleural mesothelioma: an update on biomarkers and treatment. Chest. 2009;136: 888–896.

9. Krug LM, Wozniak AJ, Kindler HL, Feld R, Koczywas M, Morero JL, et al. Randomized phase II trial of pemetrexed/cisplatin with or without CBP501 in patients with advanced malignant pleural mesothelioma. Lung Cancer. 2014;85: 429–434.

10. Scagliotti GV, Gaafar R, Nowak AK, Nakano T, van Meerbeeck J, Popat S, et al. Nintedanib in combination with pemetrexed and cisplatin for chemotherapy-naive patients with advanced malignant pleural mesothelioma (LUME-Meso): a double-blind, randomised, placebo-controlled phase 3 trial. Lancet Respir Med. 2019;7: 569–580.

11. Tsao AS, Miao J, Wistuba II, Vogelzang NJ, Heymach JV, Fossella FV, et al. Phase II Trial of Cediranib in Combination With Cisplatin and Pemetrexed in Chemotherapy-Naïve Patients With Unresectable Malignant Pleural Mesothelioma (SWOG S0905). J Clin Oncol. 2019;37: 2537–2547.

12. Zalcman G, Mazieres J, Margery J, Greillier L, Audigier-Valette C, Moro-Sibilot D, et al. Bevacizumab for newly diagnosed pleural mesothelioma in the Mesothelioma Avastin Cisplatin Pemetrexed Study (MAPS): a randomised, controlled, open-label, phase 3 trial. Lancet. 2016;387: 1405–1414.

13. Baas P, Scherpereel A, Nowak AK, Fujimoto N, Peters S, Tsao AS, et al. First-line nivolumab plus ipilimumab in unresectable malignant pleural mesothelioma (CheckMate 743): a multicentre, randomised, open-label, phase 3 trial. Lancet. 2021;397: 375–386.

14. Nowak AK, Jackson A, Sidhu C. Management of Advanced Pleural Mesothelioma-At the Crossroads. JCO Oncol Pract. 2022;18: 116–124.

15. Travis WD, Brambilla E, Nicholson AG, Yatabe Y, Austin JHM, Beasley MB, et al. The 2015 World Health Organization Classification of Lung Tumors: Impact of Genetic, Clinical and Radiologic Advances Since the 2004 Classification. J Thorac Oncol. 2015;10: 1243–1260.

16. Hmeljak J, Sanchez-Vega F, Hoadley KA, Shih J, Stewart C, Heiman D, et al. Integrative Molecular Characterization of Malignant Pleural Mesothelioma. Cancer Discov. 2018;8: 1548–1565.

17. de Reyniès A, Jaurand M-C, Renier A, Couchy G, Hysi I, Elarouci N, et al. Molecular classification of malignant pleural mesothelioma: identification of a poor prognosis subgroup linked to the epithelial-to-mesenchymal transition. Clin Cancer Res. 2014;20: 1323–1334.

18. Alcala N, Mangiante L, Le-Stang N, Gustafson CE, Boyault S, Damiola F, et al. Redefining malignant pleural mesothelioma types as a continuum uncovers immune-vascular interactions. EBioMedicine. 2019;48: 191–202.

19. Blum Y, Meiller C, Quetel L, Elarouci N, Ayadi M, Tashtanbaeva D, et al. Dissecting heterogeneity in malignant pleural mesothelioma through histo-molecular gradients for clinical applications. Nat Commun. 2019;10: 1333.

20. Mangiante L, Alcala N, Sexton-Oates A, Di Genova A, Gonzalez-Perez A, Khandekar A, et al. Multiomic analysis of malignant pleural mesothelioma identifies molecular axes and specialized tumor profiles driving intertumor heterogeneity. Nat Genet. 2023;55: 607–618.

21. Bueno R, Reblando J, Glickman J, Jaklitsch MT, Lukanich JM, Sugarbaker DJ. Pleural biopsy: a reliable method for determining the diagnosis but not subtype in mesothelioma. Ann Thorac Surg. 2004;78: 1774–1776.

22. Barbieri PG, Consonni D, Schneider M. Accuracy of pleural biopsy for the diagnosis of histologic subtype of malignant pleural mesothelioma: Necropsy-based study of 134 cases. Tumori. 2022;108: 26–32.

23. Chen X, Dong Z, Hubbell E, Kurtzman KN, Oxnard GR, Venn O, et al. Prognostic Significance of Blood-Based Multi-cancer Detection in Plasma Cell-Free DNA. Clin Cancer Res. 2021;27: 4221–4229.

24. Shen SY, Singhania R, Fehringer G, Chakravarthy A, Roehrl MHA, Chadwick D, et al. Sensitive tumour detection and classification using plasma cell-free DNA methylomes. Nature. 2018;563: 579–583.

25. Phallen J, Sausen M, Adleff V, Leal A, Hruban C, White J, et al. Direct detection of early-stage cancers using circulating tumor DNA. Sci Transl Med. 2017;9. doi:10.1126/scitranslmed.aan2415

26. Liu MC, Oxnard GR, Klein EA, Swanton C, Seiden MV, CCGA Consortium. Sensitive and specific multi-cancer detection and localization using methylation signatures in cell-free DNA. Ann Oncol. 2020;31: 745–759.

27. Cohen JD, Li L, Wang Y, Thoburn C, Afsari B, Danilova L, et al. Detection and localization of surgically resectable cancers with a multi-analyte blood test. Science. 2018;359: 926–930.

28. van der Bij S, Schaake E, Koffijberg H, Burgers JA, de Mol BAJM, Moons KGM. Markers for the non-invasive diagnosis of mesothelioma: a systematic review. Br J Cancer. 2011;104: 1325–1333.

29. Schillebeeckx E, van Meerbeeck JP, Lamote K. Clinical utility of diagnostic biomarkers in malignant pleural mesothelioma: a systematic review and meta-analysis. Eur Respir Rev. 2021;30. doi:10.1183/16000617.0057-2021

30. Cui A, Jin X-G, Zhai K, Tong Z-H, Shi H-Z. Diagnostic values of soluble mesothelin-related peptides for malignant pleural mesothelioma: updated meta-analysis. BMJ Open. 2014;4: e004145.

31. Robinson BWS, Creaney J, Lake R, Nowak A, Musk AW, de Klerk N, et al. Mesothelin-family proteins and diagnosis of mesothelioma. Lancet. 2003;362: 1612–1616.

32. Pass HI, Levin SM, Harbut MR, Melamed J, Chiriboga L, Donington J, et al. Fibulin-3 as a blood and effusion biomarker for pleural mesothelioma. N Engl J Med. 2012;367: 1417–1427.

33. Kirschner MB, Pulford E, Hoda MA, Rozsas A, Griggs K, Cheng YY, et al. Fibulin-3 levels in malignant pleural mesothelioma are associated with prognosis but not diagnosis. Br J Cancer. 2015;113: 963–969.

34. Creaney J, Francis RJ, Dick IM, Musk AW, Robinson BWS, Byrne MJ, et al. Serum soluble mesothelin concentrations in malignant pleural mesothelioma: relationship to tumor volume, clinical stage and changes in tumor burden. Clin Cancer Res. 2011;17: 1181–1189.

35. Zhang Y, Liu Y, Liu H, Tang WH. Exosomes: biogenesis, biologic function and clinical potential. Cell Biosci. 2019;9: 19.

36. Dai J, Su Y, Zhong S, Cong L, Liu B, Yang J, et al. Exosomes: key players in cancer and potential therapeutic strategy. Signal Transduction and Targeted Therapy. 2020;5: 1–10.

37. Kalluri R, LeBleu VS. The biology function and biomedical applications of exosomes. Science. 2020;367. doi:10.1126/science.aau6977

38. Yu W, Hurley J, Roberts D, Chakrabortty SK, Enderle D, Noerholm M, et al. Exosome-based liquid biopsies in cancer: opportunities and challenges. Ann Oncol. 2021;32: 466–477.

39. Mittelbrunn M, Gutiérrez-Vázquez C, Villarroya-Beltri C, González S, Sánchez-Cabo F, González MÁ, et al. Unidirectional transfer of microRNA-loaded exosomes from T cells to antigen-presenting cells. Nat Commun. 2011;2: 282.

40. Albino D, Falcione M, Uboldi V, Temilola DO, Sandrini G, Merulla J, et al. Circulating extracellular vesicles release oncogenic miR-424 in experimental models and patients with aggressive prostate cancer. Commun Biol. 2021;4: 119.

41. Toda Y, Takata K, Nakagawa Y, Kawakami H, Fujioka S, Kobayashi K, et al. Effective internalization of U251-MG-secreted exosomes into cancer cells and characterization of their lipid components. Biochem Biophys Res Commun. 2015;456: 768–773.

42. Skog J, Würdinger T, van Rijn S, Meijer DH, Gainche L, Sena-Esteves M, et al. Glioblastoma microvesicles transport RNA and proteins that promote tumour growth and provide diagnostic biomarkers. Nat Cell Biol. 2008;10: 1470–1476.

43. Skog J, Würdinger T, van Rijn S, Meijer DH, Gainche L, Sena-Esteves M, et al. Glioblastoma microvesicles transport RNA and proteins that promote tumour growth and provide diagnostic biomarkers. Nat Cell Biol. 2008;10: 1470–1476.

44. Al-Nedawi K, Meehan B, Micallef J, Lhotak V, May L, Guha A, et al. Intercellular transfer of the oncogenic receptor EGFRvIII by microvesicles derived from tumour cells. Nat Cell Biol. 2008;10: 619–624.

45. Zhou X, Xie F, Wang L, Zhang L, Zhang S, Fang M, et al. The function and clinical application of extracellular vesicles in innate immune regulation. Cell Mol Immunol. 2020;17: 323–334.

46. Kamerkar S, LeBleu VS, Sugimoto H, Yang S, Ruivo CF, Melo SA, et al. Exosomes facilitate therapeutic targeting of oncogenic KRAS in pancreatic cancer. Nature. 2017;546: 498–503.

47. Kraft A, Kirschner MB, Orlowski V, Ronner M, Bodmer C, Boeva V, et al. Exploring RNA cargo in extracellular vesicles for pleural mesothelioma detection. BMC Cancer. 2025;25: 212.

48. Buske FA, Bodén M, Bauer DC, Bailey TL. Assigning roles to DNA regulatory motifs using comparative genomics. Bioinformatics. 2010;26: 860–866.

49. Xu Y-F, Xu X, Gin A, Nshimiyimana JD, Mooers BHM, Caputi M, et al. SRSF1 regulates exosome microRNA enrichment in human cancer cells. Cell Commun Signal. 2020;18: 130.

50. Xia H-F, Wang X-L, Zhang H-J, Wang K-M, Zhang L-Z, Yang Y, et al. PCBP2-dependent

secretion of miRNAs via extracellular vesicles contributes to the EGFR-driven angiogenesis. Theranostics. 2025;15: 1255–1271.

51. Fu Y, Huang B, Shi Z, Han J, Wang Y, Huangfu J, et al. SRSF1 and SRSF9 RNA binding proteins promote Wnt signalling-mediated tumorigenesis by enhancing β-catenin biosynthesis. EMBO Mol Med. 2013;5: 737–750.

52. Szklarczyk D, Kirsch R, Koutrouli M, Nastou K, Mehryary F, Hachilif R, et al. The STRING database in 2023: protein-protein association networks and functional enrichment analyses for any sequenced genome of interest. Nucleic Acids Res. 2023;51: D638–D646.

53. Villarroya-Beltri C, Gutiérrez-Vázquez C, Sánchez-Cabo F, Pérez-Hernández D, Vázquez J, Martin-Cofreces N, et al. Sumoylated hnRNPA2B1 controls the sorting of miRNAs into exosomes through binding to specific motifs. Nat Commun. 2013;4: 2980.

54. Elkahwagy DM, Kiriacos CJ, Sobeih ME, Khorshid OMR, Mansour M. The lncRNAs Gas5, MALAT1 and SNHG8 as diagnostic biomarkers for epithelial malignant pleural mesothelioma in Egyptian patients. Sci Rep. 2024;14: 4823.

55. Robey RW, Pluchino KM, Hall MD, Fojo AT, Bates SE, Gottesman MM. Revisiting the role of ABC transporters in multidrug-resistant cancer. Nat Rev Cancer. 2018;18: 452–464.

56. Wang G, Xu D, Zhang Z, Li X, Shi J, Sun J, et al. The pan-cancer landscape of crosstalk between epithelial-mesenchymal transition and immune evasion relevant to prognosis and immunotherapy response. NPJ Precis Oncol. 2021;5: 56.

57. Keenan AB, Torre D, Lachmann A, Leong AK, Wojciechowicz ML, Utti V, et al. ChEA3: transcription factor enrichment analysis by orthogonal omics integration. Nucleic Acids Res. 2019;47: W212–W224.

58. Nie J-H, Li T-X, Zhang X-Q, Liu J. Roles of Non-Coding RNAs in Normal Human Brain Development, Brain Tumor, and Neuropsychiatric Disorders. Noncoding RNA. 2019;5. doi:10.3390/ncrna5020036

59. Bao X, Lee YS, Lee I. Small non-coding RNAs in diseases. Frontiers Media SA; 2023.

60. Zhu L, Li J, Gong Y, Wu Q, Tan S, Sun D, et al. Exosomal tRNA-derived small RNA as a promising biomarker for cancer diagnosis. Mol Cancer. 2019;18: 74.

61. Reale A, Khong T, Spencer A. Extracellular Vesicles and Their Roles in the Tumor Immune Microenvironment. J Clin Med. 2022;11. doi:10.3390/jcm11236892

62. Oehl K, Kresoja-Rakic J, Opitz I, Vrugt B, Weder W, Stahel R, et al. Live-Cell Mesothelioma Biobank to Explore Mechanisms of Tumor Progression. Front Oncol. 2018;8: 40.

63. Chen S. Ultrafast one-pass FASTQ data preprocessing, quality control, and deduplication using fastp. Imeta. 2023;2: e107.

64. McInnes L, Healy J, Melville J. UMAP: Uniform Manifold Approximation and Projection for Dimension Reduction. arXiv [stat.ML]. 2018. doi:10.48550/ARXIV.1802.03426

65. Love MI, Huber W, Anders S. Moderated estimation of fold change and dispersion for RNA-seq data with DESeq2. Genome Biol. 2014;15: 550.

66. Hänzelmann S, Castelo R, Guinney J. GSVA: gene set variation analysis for microarray and RNA-seq data. BMC Bioinformatics. 2013;14: 7.

67. Pinheiro C, Guilbert N, Lippens L, Roux Q, Boiy R, Fischer S, et al. Identification and validation of extracellular vesicle reference genes for the normalization of RT-qPCR data. J Extracell Vesicles. 2024;13: e12421.

68. Antonio Colaprico, Tiago Chedraoui Silva, Catharina Olsen, Luciano Garofano, Davide Garolini, Claudia Cava, Thais Sabedot, Tathiane Malta, Stefano M. Pagnotta, Isabella Castiglioni, Michele Ceccarelli, Gianluca Bontempi, Houtan Noushmehr. TCGAbiolinks. Bioconductor; 2017. doi:10.18129/B9.BIOC.TCGABIOLINKS

69. Aran D, Hu Z, Butte AJ. xCell: digitally portraying the tissue cellular heterogeneity landscape. Genome Biol. 2017;18: 220.